RSC Advances

ROYAL SOCIETY OF CHEMISTRY

www.rsc.org/advances

A stable Ni/SBA-15 catalyst prepared by the ammonia evaporation method for dry reforming of methane

Qiulin Zhang*, Mingzhi Wang, Tengfei Zhang, Yiru Wang, Xiaosu Tang, Ping Ning

Faculty of Environmental Science and Engineering, Kunming University of Science and Technology. Kunming, 650500, P.R. China

* Corresponding author. E-mail: qiulinzhang_kmust@163.com

Abstracts: A stable Ni/SBA-15 catalyst was prepared by ammonia evaporation (Ni-AE) method for dry reforming of methane. The characterization results exhibited that the highly dispersed and uniformly distributed Ni nanoparticles with strong metal-support interactions can be obtained by ammonia evaporation method. The presence of Ni phyllosilicate was crucial to obtain the Ni nanoparticles with size of 3.2-5.2 nm after reduction by H_2, which were smaller and exhibited narrower size distribution than in the sample prepared by impregnation (Ni-IM). Dry reforming of methane reactivity results showed no observed decrease of activity for Ni-AE even reacted at 800 °C for 100 min or 700 °C for 100 h, while the Ni-IM presented obvious decrease at the same conditions. TEM images of spent Ni-AE catalyst further confirmed that the Ni nanoparticles were highly dispersed, and the weight loss of Ni-AE (2.09%) revealed by the TG curves is much lower than that of Ni-IM sample (24.16%). The strong metal-support interactions deriving from Ni phyllosilicate were mainly responsible for resistant to the coking and sintering.

Keywords: Methane, reforming, coking, sintering, metal-support interactions

1. Introduction

In recent years, dry reforming of methane (DRM) has received increasing attention for syngas production[1-3] and chemical energy transmission[4]. This process enables syngas production with a lower H_2/CO ratio close to 1, which is more adequate for Fischer-Tropsch synthesis.[2] Besides, it shows a 20% lower operating cost compared to the commercial steam reforming of methane (SRM) in spite of the deactivation issues[5]. In addition, it is also an effective route to alleviate global warming by utilizing the two greenhouse gases. As the widely studied catalytic systems, the noble Group VIII metals containing catalysts such as Pa, Pt, Ru, Ir, et al.[3] are highly active

towards DRM. However, the application of noble metals catalyst is confined by the high cost and limited supply. Thus, the most extensively used catalysts for dry reforming of methane are non-noble metal, Ni-based catalysts. Unfortunately, they are prone to carbon deposition during reforming process, which causes the catalyst deactivation or even breakdown of the catalyst structure.[6-7] On the other hand, the DRM processes are generally favored at temperatures higher than 700 °C. This reaction condition typically causes the sintering of metal nanoparticles due to atomic migration and crystallite migration.[8] Especially during the long-term DRM reaction, the catalysts deactivation due to loss metal surface area by coking and sintering was usually unable to avoid.

Many attempts have been made to suppress coking and sintering over dry reforming Ni-based catalysts. One feasible solution is to design and synthesize catalysts with strong metal-support interactions (SMSI). For this purpose, introducing a second metal on nickel catalysts such as alkali[9-10], alkaline earth[11], transition metal[12], or small amounts of noble metals[13] was widely researched. Although some promoters (Ag, Mn, Cu, K) can enhance the long-term catalytic stability, the initial catalytic activity reduced significantly due to the decreased surface dispersions of metal.[14-15] In addition, its extra cost is undesirable for practical industrial uses. Another way to achieve a catalyst with SMSI is to confine Ni particles in defined structures. The confinement effect will result in an improved resistance to coking and sintering. Among these structures, order mesoporous silica SBA-15 possesses outstanding properties such as high specific surface area, excellent thermal stability, tunable porosity and uniform two-dimensional hexagonal pore structure with thick pore walls. Thus it is widely used as a superior host to disperse and confine metal nanoparticles. However, the catalytic stabilities for high-temperature reaction were still not desirable, because the interaction between the nickel species and support was not strong enough to stabilize the nickel species under a long-term reaction. The previous results showed that Ni particles could sinter and migrate out of the mesoporous channels to the exterior surface of SBA-15 at the high-temperature condition, resulting in heavier sintering.[16] For the conventional impregnation method, the obtained NiO usually present in a form which is very similar to bulk oxide, and it is hard to be driven into the channel. Thus, only weak interactions occur between the active phase and the support.[17] As a result, the Ni particle is easier to sinter. More seriously, the sintered Ni nanoparticles lead to fast carbon formation. Recently, a novel preparation called

ammonia evaporation (AE) method that based on homogeneous deposition-precipitation (HDP) has been reported to enhance metal-support interactions. It is a technique by which a solvated metal precursor disperses onto the surface of a suspended support by ammonia evaporation[18-19]. Recently, a series of Cu/SiO_2 catalysts prepared by ammonia evaporation have been investigated for hydrogenation of oxalates to ethylene glycol (EG) by Yin et al. and Ma et al.[20-24]. It was reported that the strong metal-support interactions are crucial for the high catalytic activity and stability. Particularly, the formation of copper phyllosilicate by the AE method makes the copper highly dispersed after reduction.[19] However, only limited work was reported regarding the improvement of coking and sintering resistance of the Ni catalyst for DRM.

In the present work, the ammonia evaporation (AE) method was employed to prepare a highly stable catalyst for harsh dry reforming reaction. The physicochemical properties of Ni/SBA-15 were characterized by multiple techniques. The resistance to coking and sintering of Ni/SBA-15 catalysts toward the dry reforming of methane was studied. The stability of Ni particles was thoroughly evaluated by dry reforming of methane reaction at 800 °C for 100 min and 700 °C for 100 h, respectively.

2. Experimental

2.1. Catalyst preparation

SBA-15 were prepared according to the previously reported methods described by Zhao et al.[25TT] The Ni/SBA-15 catalysts were prepared by the AE method, a defined amount of $Ni(NO_3)_2 \cdot 6H_2O$ adjusted to Ni/Si ratio = 0.06 in the final catalysts, and 6 ml of 25-28 wt.% ammonia aqueous solution dissolved in 44 ml deionized water were mixed and stirred for 10 min, then 2 g SBA-15 was added in and stirred at 80 °C for 4 h. During the ammonia evaporation process, the initial pH of the suspension was decreased from 11-12 to 7. After that, the obtained precipitates were filtrated and washed with deionized water three times and dried at 120 °C overnight. The catalyst was obtained after calcined in static air at 400 °C for 4 h (denoted as Ni-AE). For comparison, Ni/SBA-15 was also prepared by conventional incipient wetness impregnation (denoted as Ni-IM).

2.2. Catalyst characterization

Nitrogen adsorption-desorption isotherms were measured at -196 °C on a Micromeritics TriStar

Ⅱ3020 static volumetric instrument. Prior to the measurements, the samples were degassed at 300 °C for 5 h under high vacuum. X-ray diffraction (XRD) measurements were carried out on a Bruker D8 Advance X-ray diffraction meter using Ni-filtered Cu Kα radiation (λ = 0.15406 nm), operated at 40 kV and 40 mA with a scanning speed (2θ) of 1° min^{-1}. X-ray photoelectron spectroscopy (XPS) experiments were carried out on a thermo ESCALAB 250XI equipment. All the electron binding energies were calibrated using C1s peak at 284 eV as the reference. TEM and high resolution TEM (HRTEM) of the samples were measured on a FEI Tecnai G20 transmission electron microscope, which use an accelerating voltage of 200 kV. Thermogravimetric-differential scanning calorimetry (TG-DSC) measurements were carried out on a SDT Q600 thermogravimetric analyzer from room temperature to 900 °C at a rate of 10 °C/min under air atmosphere. Hydrogen temperature-programed reduction (TPR) was carried out on gas chromatography equipped with a TCD detector. Before the test, 50 mg samples were activated at 400 °C for 40 min in N_2 (30 ml/min). All TPR runs were performed from 100 to 900 °C under 5% H_2/Ar with a heating rate of 8 °C/min.

2.3. Catalytic reaction experiments

Catalytic activity tests were carried out in a continuous down-flow quartz fixed-bed reactor (i.d. 6 mm) under atmospheric pressure. Typically, 50 mg of catalysts were loaded on a quartz wool bed. Prior to the reaction, the catalysts were reduced *in situ* at 700 °C for 1 h under pure hydrogen (20 ml/min). A reaction mixture of CH_4 and CO_2 (molar ratio = 1: 1) without dilution was fed with a gas hourly space velocity (GHSV) of 36 000 ml/g·h. The activity of catalysts was tested in the temperature range of 600-800 °C at a 50 °C increment. When the temperature rose to the desired level, maintained for 30 min before the test. Particularly, the temperature was maintained at 800 °C for 100 min before the temperature cool down. For long-term stability test experiments, the reaction temperature was kept constant at 700 °C for 100 h otherwise the same condition. The product was analyzed using an on-line gas chromatograph (Fuli 9790) equipped with a TDX-01 column and a thermal conductivity detector (TCD).

3. Results and discussion

3.1. Physicochemical properties of the catalysts

3.1.1. Textural properties

Nitrogen physisorption results of Ni/SBA-15 and the support were showed in Fig. 1 and the textural parameters were summarized in Tab. 1

Tab. 1 Physicochemical properties of Ni/SBA-15 catalysts and SBA-15

Sample	Surface area (m^2/g)[a]	Average pore diameter (Å)[b]	Pore volume (cm^3/g)[b]	Ni particle size (nm)[c]
SBA-15	678.6539	63.907	0.861136	-
Ni-IM	555.2777	65.786	0.741342	6.21
Ni-AE	412.2894	87.240	0.781283	4.09

a Calculated by BET method

b Calculated by BJH method

c Ni particle size: Measured by TEM for catalysts reduced at 700 °C by H_2 for 1 h

As shown in Tab. 1, introduction of nickel via IM or AE method remarkably decreased the specific surface area and the pore volume of SBA-15. It suggested partial plugging of microporous by metal oxide clusters, which were confined in the primary mesoporous channels. Moreover, compared with Ni-IM catalyst, the Ni-AE catalyst showed the tilt of the hysteresis loop of N_2 adsorption-desorption isotherms, corroborating with the partial destruction of the ordered structure. There were two reasonable explanations accounting for this phenomenon. One of them was that small part of the SBA-15 transfer into amorphous non-ordered silica[26], which was due to the treatment in basic solution during the synthesis process[27]. Another reason was attributed to the dissolution of the silica wall of SBA-15 for the formation of nickel phyllosilicate[28].

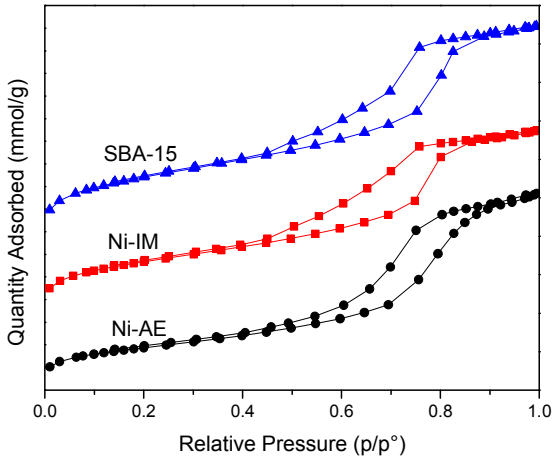

Fig. 1 N_2 adsorption/desorption isotherms for calcined SBA-15 and Ni/SBA-15 samples

3.1.2. XRD

XRD patterns of the calcined Ni-AE and Ni-IM samples were shown in Fig. 2. In the small angle XRD patterns, for both of Ni-AE and Ni-IM samples, three peaks at 2θ = 0.9°, 1.5°, and 1.8° can be discerned with the strongest one corresponding to (100) diffraction followed by two well-resolved (110) and (200) peaks, which can be indexed to a hexagonal lattice. It demonstrated that the structural integrity has been retained after Ni loading by different prepared methods. In the wide angle XRD patterns, there was a broad peak around 2θ = 15–30° both on the calcined Ni-AE and Ni-IM should be attributed to SiO_2 (SBA-15). Obviously, there were four intensive diffraction peaks at 2θ = 37.2°, 43.3°, 62.9°, 75.4° corresponding to the (101), (012), (110) and (113) reflections of NiO (JCPDS No. 44-1159) were detected on the calcined Ni-IM. In contrast, no peak of crystalline NiO was detected on calcined Ni-AE, suggesting that the NiO particles were highly dispersed in or on SBA-15. The peaks were discernable at 2θ = 34.1°, 36.7°, and 60.5°, and were clearly assigned to (200), (202), and (060) diffractions of nickel phyllosilicate (JCPDS No. 49-1859), respectively. The ill-crystallized nickel phyllosilicate result was consistent with the Burattin's studies.[29] They asserted that the long time deposition-precipitation (>4 h) make the Ni/SiO_2 sample form ill-crystallized 1:1 nickel phyllosilicate on silica.

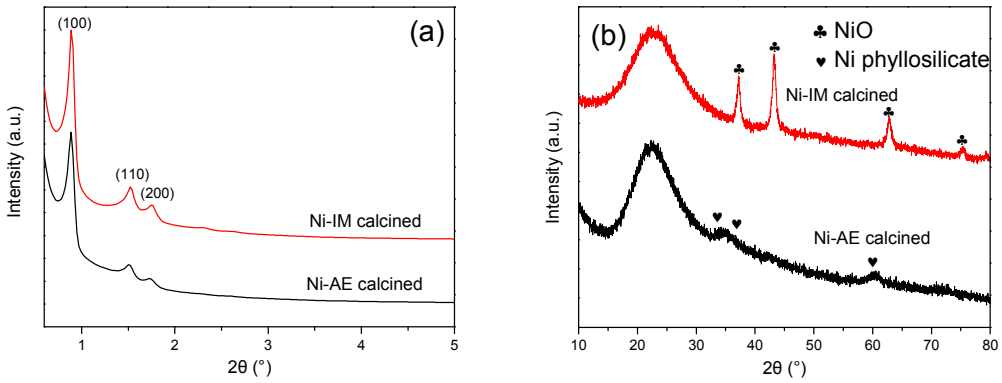

Fig. 2 Small-angle (a) and wide angle (b) XRD patterns for calcined Ni/SBA-15 samples

3.1.3. H_2-TPR

TPR profiles of Ni/SBA-15 samples were displayed in Fig. 3. The small shoulder reduction peak at 254 and 272 °C may reflect the presence of bulk NiO particles.[30] Both of them were very weak due to the low loading. The next two peaks, 362 and 416 °C for Ni-IM and 371 and 490 °C for Ni-AE, should be assigned to the reduction of NiO in channel and external surface,

respectively.[31-33] Due to confinement effect, the metal-support interactions in the channel were much stronger than that outside. Broad peaks at 679 °C indicated that main reduction occurred at T＞550 °C, it should be ascribed to the reduction of 1:1 nickel phyllosilicate. Based on the results of the peak areas, the Ni species in Ni-AE mainly existed in the form of nickel phyllosilicate instead of NiO.

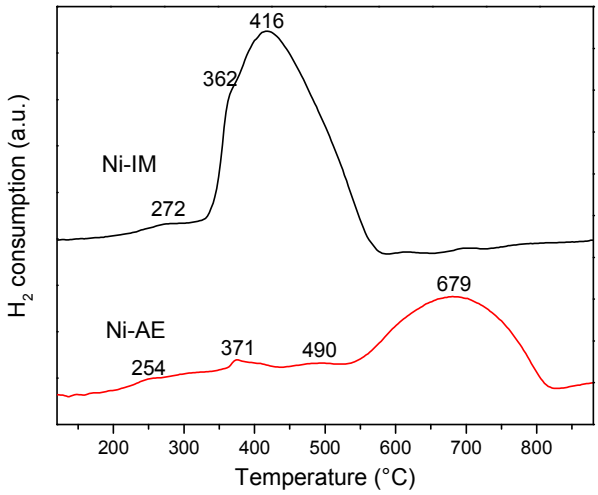

Fig. 3 H_2-TPR profiles of Ni/SBA-15 samples.

As it has been identified in many previous studies,[34] Ni phyllosilicates are generally formed through hexaamminenickel nucleation and growth on the silica surface under a hydrothermal condition. It is formed via hydrolytic adsorption to evolve into Si-O-Ni bonds and subsequent steps of hetero-condensation or polymerization. By long time deposition-precipitation, the nickel phase is mainly a 1:1 nickel phyllosilicate.[35-36]

3.1.4. XPS

The supported Ni(II) phase was further studied by XPS. The Ni 2p3/2 peak binding energy shifts from 855.4 to 856.85 eV, demonstrating the existence of interaction between the metal and support in Ni-AE sample. The difference of binding energies $\Delta E_{Ni\text{-}Si}$ = Ni 2p3/2 - Si 2P is used as a specific indicator seem reasonable due to the reduced calibration problem.[37] Based on Coenen's work, the bonding of nickel as silicates give the $\Delta E_{Ni\text{-}Si}$ values between 753.2 and 753.6 eV, and the values are in line with amounts of nickel silicate. However other nickel species exhibit significantly lower differences. Here, the difference for Ni-AE catalysts was 753.26 eV ($\Delta E_{Ni\text{-}Si}$ = 856.85 – 103.59), which was coincided with the Ni silicate. For Ni-IM catalyst, lower difference

of 751.59 eV ($\Delta E_{Ni\text{-}Si}$ = 855.4 – 103.81) was found, suggesting that no Ni silicate was formed. Notably, the ratio of Ni/Si for Ni-AE (Ni/Si = 0.1936) was several times higher than the Ni-IM (Ni/Si = 0.0321), indicating a relatively high specific Ni^0 surface area.[38-39]

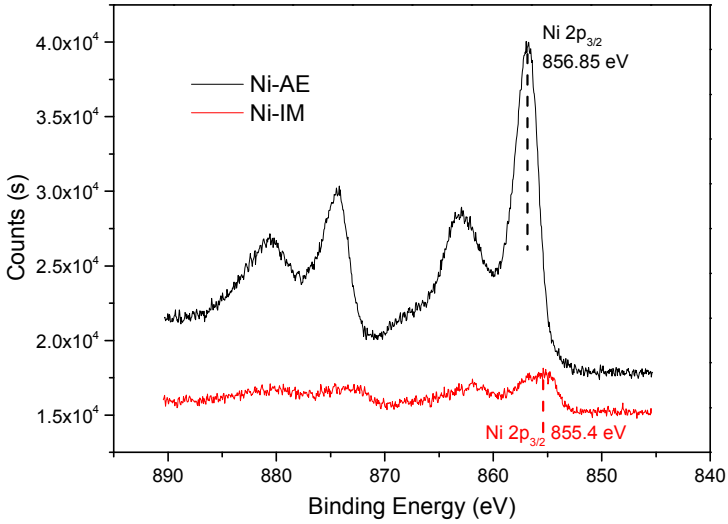

Fig. 4 XPS spectra in Ni 2p region for the calcined Ni/SBA-15 samples.

3.1.5. TEM

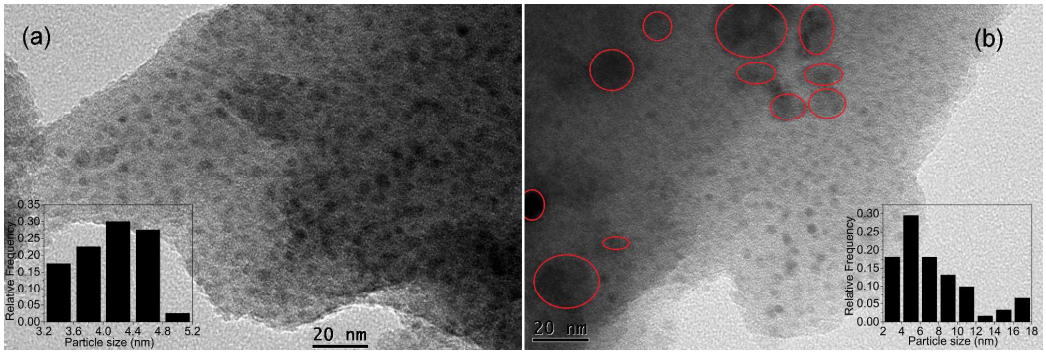

Fig. 5 TEM images and nickel particle size distributions of the reduced Ni/SBA-15 catalysts: (a), Ni-AE sample; (b), Ni-IM sample.

Ni particle morphology and particle size distribution was determined from TEM. As shown in Fig. 5, there was a broad range of particle size from 2.47 to 17.1 nm for the reduced Ni-IM sample. Some bulky Ni particles were clearly visible in the TEM images. These particles may be formed during calcination or reduction. Conversely, the Ni-AE sample showed much narrower particle size distribution of 3.05-5.17 nm with an average diameter of 4.09 nm. It was widely believed that the stronger the metal-support interaction, the smaller the metal particle size formed by

reduction.[40-42] The uniform distribution should attribute to sufficient interaction between nickel aqua ammine complex ions and surface silanol groups in the aqueous phase. The highly dispersed Ni-AE sample shown by TEM images was consistent with the XRD result.

3.2. Comparison of initial catalytic activity and high-temperature catalytic stability

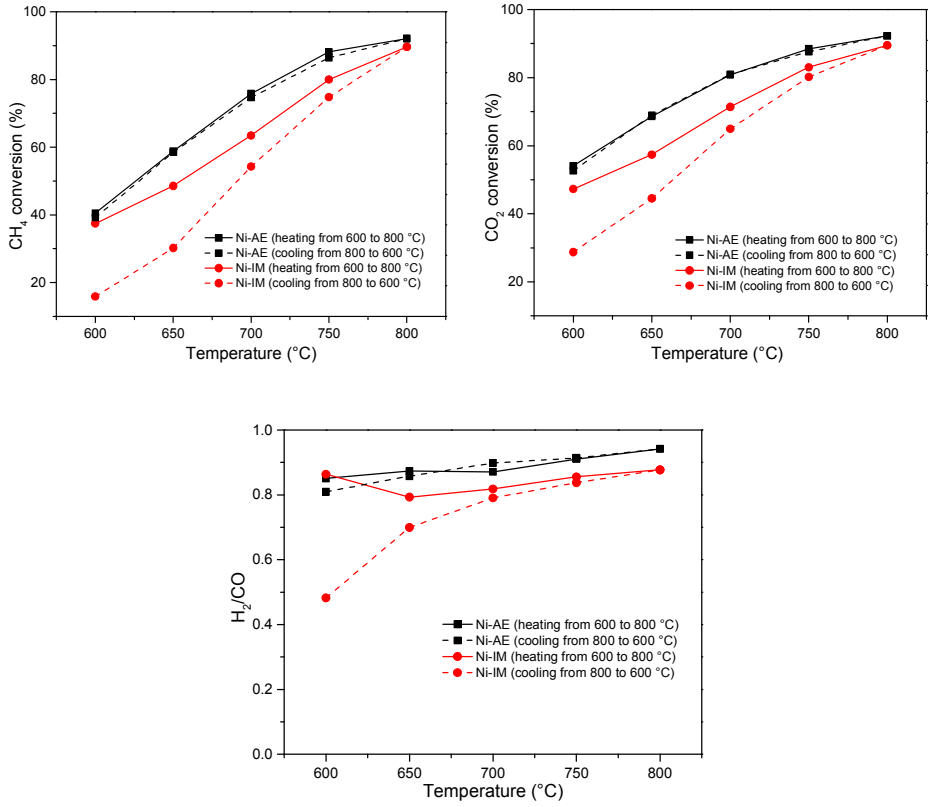

Fig.6 Effect of reaction temperature on the catalytic performance over Ni/SBA-15 catalysts (CH_4/CO_2 = 1, GHSV = 36 000 ml/(g·h), 1 atm).

The catalytic activity and high-temperature catalytic stability of the catalysts were investigated in a fixed-bed reactor. Fig. 6 showed the initial catalytic performances expressed as the conversions of CH_4, CO_2 and the H_2/CO ratios of various catalysts at different temperatures. As expected, the conversions of both CH_4 and CO_2 increase with reaction temperature. It should be mentioned that the CO_2 conversions were higher than of the methane conversion for all investigated temperature stages due to the occurrence of simultaneous reverse water gas-shift (RWGS) reaction (eq. (1))[43]. Meanwhile, the product of H_2 was partly consumed, leading to the relatively lower ratio than that of the stoichiometric ratio. Furthermore, it could also be observed that the gap between CO_2 conversion and CH_4 conversion decreased as the reaction temperature increased. This could be

due to the fact that the RWGS reaction was suppressed at high temperatures.

$$CO_2 + H_2 \Leftrightarrow CO + H_2O \qquad \Delta H_{298^\circ} = 41 \text{ kJ/mol} \qquad (1)$$

Obviously, the Ni/SBA-15 prepared by AE method showed the better catalytic activity and selectivity compared with that prepared by IM method. The excellent catalytic activity of Ni-AE should be closely associated with the improved dispersion of Ni active sites by AE method.

In order to estimate the sintering resistance ability of Ni/SBA-15 catalysts at high-temperature, the catalysts were maintained at 800 °C for 100 min. When the reaction temperature declines, the Ni-AE almost kept all the initial activity while the Ni-IM lost considerable of them. For the Ni-AE, the two lines (heating from 600 to 800 °C and cooling from 800 to 600 °C) almost coincided. However, the Ni-IM presented a considerably wider hysteresis loop, indicating that severe deactivation occurred on Ni-IM during the reaction. The main reason for their deactivation should be attributed to the sintering of catalyst. It can be noted that the catalysts still retained most of its initial activity at high temperatures in spite of sintering has formed. This might be due to the CH_4, CO_2 conversions at high temperatures was mainly affected by thermodynamics factors. However, loss metal surface area by sintering was usually irreversible.[44] When the temperature cool down, the activity declined sharply due to sintering.

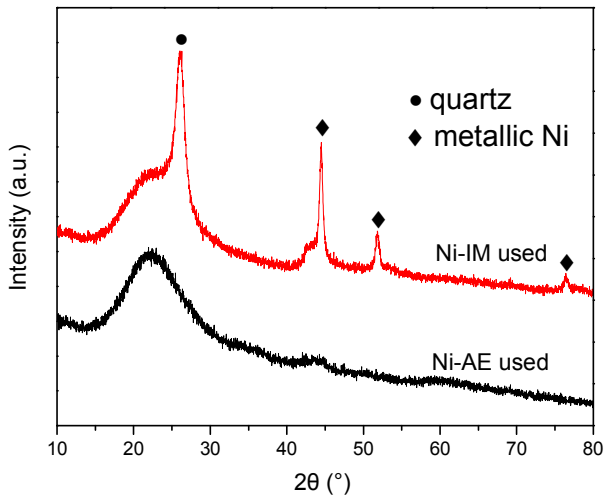

Fig. 7 Wide angle XRD patterns of the used Ni/SBA-15 catalysts

XRD profiles of the activity-tested catalysts were shown in Fig. 7. For Ni-IM, the crystal structure of the catalyst was different as compared to the calcined catalysts. An obvious peak attributing to the quartz (JCPDS No.11-0252) was observed at 2θ = 26.2°, which was transformed from

amorphous silica.[45] However, no crystalline SiO_2 phase was detected on Ni-AE. It suggested that the impregnation method was unfavorable for the thermal stability of SBA-15. For Ni-IM, three peaks at 2θ = 44.5°, 51.8°, 76.4° corresponding to the metallic Ni (JCPDS No.04-0850). Nevertheless, the crystalline Ni was still could not be detected for Ni-AE. This further indicated that the Ni nanoparticles were highly dispersed even after high temperature reforming reaction at 800 °C. It should be noted that coking on both of the catalysts was too slight to be detected. Because, both the coke formation routes (eq. (2) and (3)) were suppressed at 800 °C.

$$CH_4 \Leftrightarrow 2H_2 + C \qquad \Delta H_{298^\circ} = 75 \text{ kJ/mol} \qquad (2)$$

$$2CO \Leftrightarrow C + CO_2 \qquad \Delta H_{298^\circ} = -171 \text{ kJ/mol} \qquad (3)$$

3.3. Comparison of long-term catalytic stability

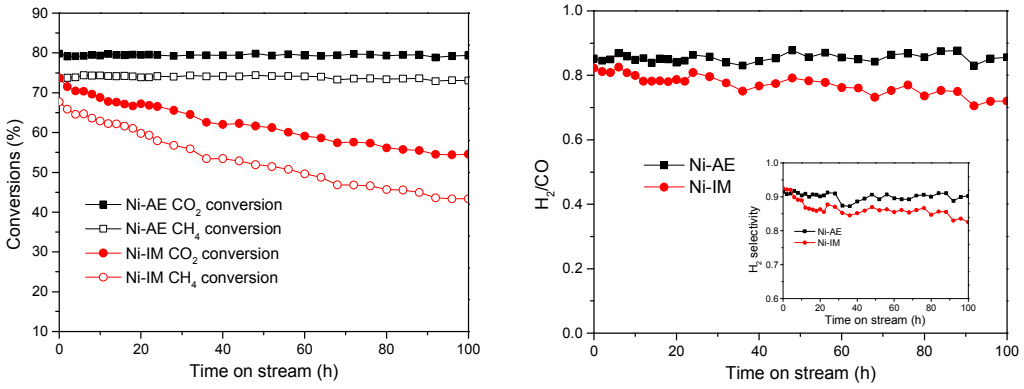

Fig. 8 The long-term catalytic stability in the dry reforming of methane over Ni/SBA-15 catalysts at 700 °C (CH_4/CO_2 = 1, GHSV = 36 000 ml/(g_{cat}·h), 1 atm).

The long-term catalytic stabilities of the catalysts were examined during a 100 h DRM reaction period under typical reaction conditions. As shown in Fig. 8, Ni-AE exhibited higher CH_4 and CO_2 conversions and H_2/CO ratio than Ni-IM. No apparent deactivation for Ni-AE was observed in Fig. 8. However, the activity of Ni-IM decreased linearly with time on stream. More than that, its conversions could not remain constant even during the first few hours. Meanwhile, the H_2/CO ratio also decreased with time on stream, it meant that the side reaction became serious. The fluctuation of the H_2/CO ratios implied that the carbon deposition reaction (eq. (2) and (3)) and coke elimination reaction (eq. (4) and (5)) took place by turns.[46]

$$C + H_2O \Leftrightarrow CO + H_2 \qquad (4)$$

$$C + CO_2 \Leftrightarrow 2CO \qquad (5)$$

The excellent catalytic stability over Ni-AE catalyst lied in the formation of Ni phyllosilicates, as it confirmed by XRD, XPS. Due to the lamellar structure of Ni phyllosilicates, the Ni^{2+} were isolated and surrounded by silica, which would lead to the formation of highly dispersed and homogeneous distributed Ni nanoparticles. Meanwhile, Ni nanoparticles were stabilized by strong metal-support interactions or metal oxide-support interactions through Si-O-Ni-O-Si bonding. Thus, the long-term catalytic performance was greatly improved.

3.4. Analysis of catalyst deactivation

Fig. 9 depicts thermogravimetric (TG) and differential scanning calorimetry (DSC) characterizations for the spent catalysts after the endurance test. The TG curves were used to show the weight loss resulting from the removal of carbon. It should be mentioned that low-temperature weight loss at approximately 100 °C was associated with the pronounced desorption of moisture. The slight weight rise around 300 °C caused by the oxidation of metallic Ni particles was negligible since the nickel loading was quite low and similar for both of the samples. Notably, the TG curves showed that the weight loss of the coke over Ni-AE sample was much lower than that of Ni-IM sample. The excellent coke resistance properties of Ni-AE should attribute to the strong metal-support interactions resulting from the ammonia evaporation method used. Previous work has shown that the strong metal-support interactions are conducive to formation of smaller metal particles with high dispersion.[39-42] As a result, the formation of carbon was generally suppressed by the small Ni particles.

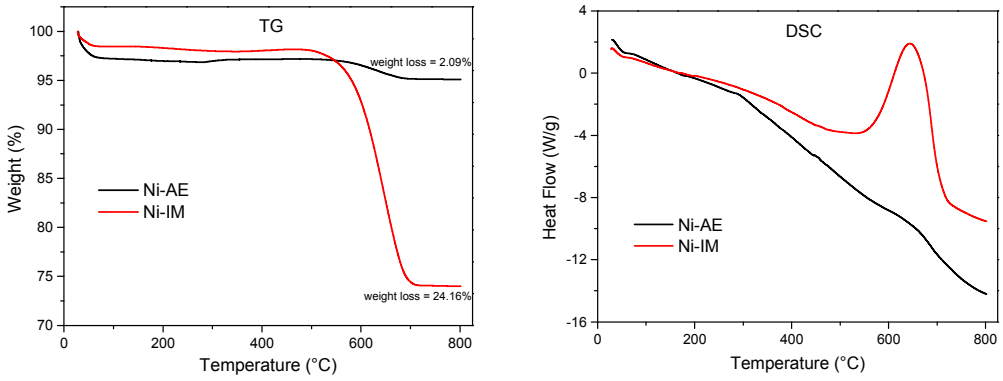

Fig. 9 TG and DSC curves of the 100 h stability tested Ni/SBA-15 catalysts

The DSC profiles exhibited that the carbon species could be burned up in a temperature range between 240 and 730 °C. Two exothermic peaks around 300 and 630 °C were observed, indicating

that at least two kinds of carbon species were formed on the catalysts. The strong peak at a relatively high temperature could be attributed to the oxidation of coke deposits in the filament carbon (also called carbon nanotubes or nanofibers)[45], and the weak peaks at low temperatures were ascribed to the oxidation of amorphous carbon, which burns easier due to low density of deposited carbon structures.[47] For both of the catalysts, the amount of filament carbon was much higher than that of the amorphous carbon. Hence, it can be concluded that the carbon deposited on Ni-AE and Ni-IM were predominantly filament carbon.

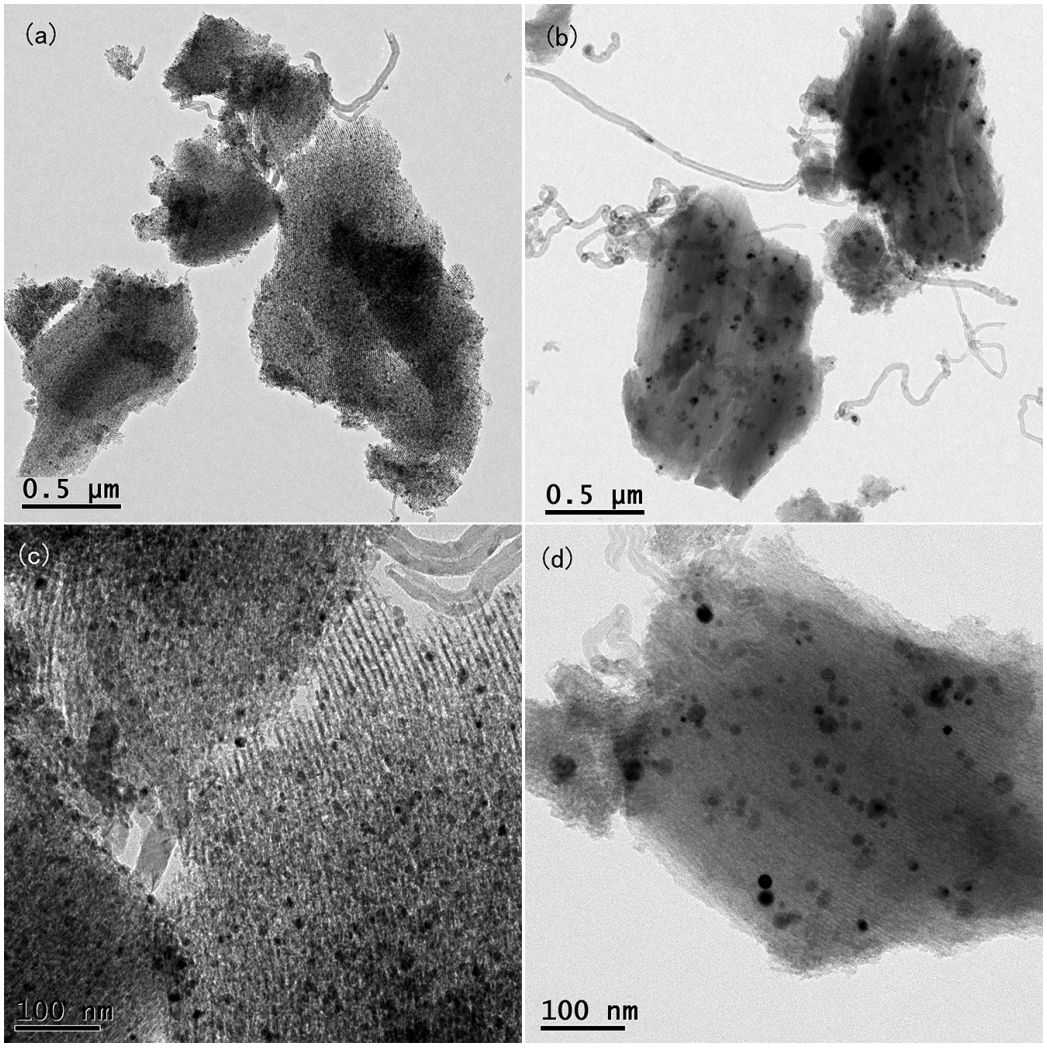

Fig. 10 TEM images of the Ni-AE (a) (c) and Ni-IM (b) (d) catalysts after 100 h stability test.

The carbon formation and Ni metal sintering of the spent catalysts was also examined using TEM, which is shown in Fig. 10. For both of the catalysts, the observed deposited carbon morphology over the spent catalysts was mainly the filament carbon. Compared with the Ni-IM catalyst, the amount of coke for Ni-AE was much lower. Although the deposited carbon over spent

Ni-AE could not be neglected (Fig. 10(a)), the Ni-AE showed relatively good catalytic stability with time on stream. This meant that the carbon deposited on the surface of Ni-AE has no significant effect on its activity and stability. It is generally accepted in the literature that most of the filamentous carbon over the spent catalysts has no influence on activity.[48-49] This theory is well-known with the growth mechanism suggested by J. K. Nørskov, i.e. carbon nanotubes developed initially at step edges on nickel surfaces[50] and continuously lifted up nickel metal clusters following the tip-growth mechanism[51]. This phenomenon could be observed by TEM. As shown in Fig. 11, the observed coke morphology over the spent catalysts was primarily the filament carbon. Obviously, heavy coking by filamentous carbon was observed for the spent Ni-IM, while the Ni-AE was slight. From the TEM results, at least three types of filament carbon formed during the stability test were observed: i. Filament carbon without Ni nanoparticle on the tip (Fig. 11(b)); ii. Filament carbon with Ni nanoparticle on the tip (Fig. 11(c)); iii. Filament carbon embedded Ni nanoparticle inside tubes (Fig. 11(d)). As shown in Fig. 11, Ni-IM surface coke residue was mainly the first and second type. For these filament carbons, the Ni active sites remain uncovered or partly encapsulated, they were still accessible to the reactants. Therefore, deactivation did not occur by them. The third type filament carbon completely enwrapped the Ni particles. As a result, the Ni active centers were not accessible, which finally caused the deactivation.

On the other hand, there was no carbon nanotubes were observed among the mesoporous channel for the both catalysts, and the coking were mainly occurred at the edge of channel or outside the channel. This implied that the “confinement effect” of the mesoporous channels effectively inhibited the growth of filament carbon.[46,52] For the Ni-AE catalyst, besides the confinement effect driven form the SBA-15, the homogeneous distributed Ni particles with smaller size was the main reason for its resistance to coke formation. It was also worth mentioning that no obvious amorphous carbon was observed. This could be understood that the formation of amorphous carbon in the mesoporous channel was easily eliminated by CO_2 and steam.[53]

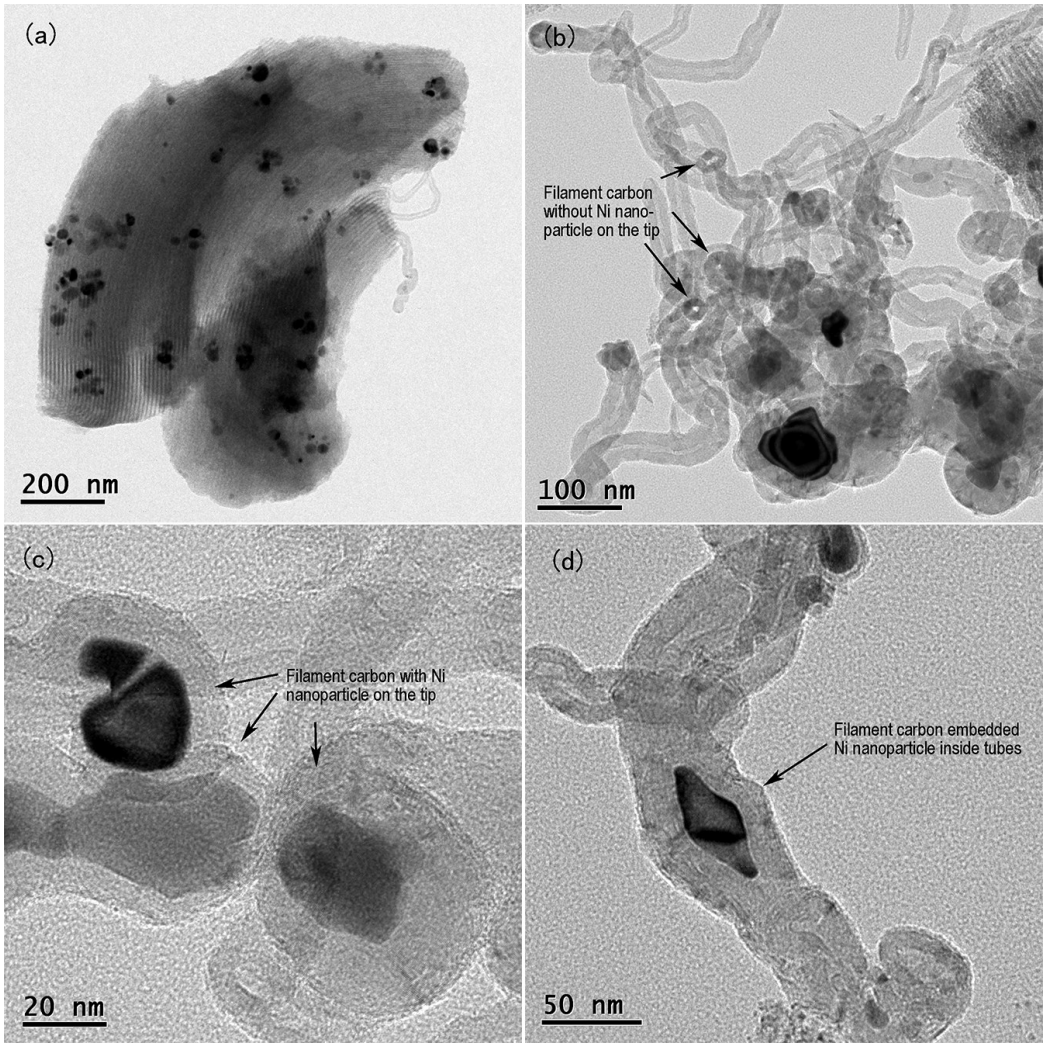

Fig. 11 Morphology of sintering and coking for Ni-IM catalyst after 100 h stability test.

The severe sintering for Ni-IM was also observed in Fig. 11(a). A majority of Ni particles exhibited a large size above 30 nm. In Fig. 11(b), a large Ni particle with a size above 60 nm was found. As can be imagined，considerable Ni metal surface active sites were lost due to the agglomeration of Ni particle. On the contrary, the Ni particles were still highly dispersed after 100 h long-term reaction at 700 °C (Fig. 10(c)). The outstanding resistance to sintering for Ni-AE was further confirmed by XRD (Fig.12). In comparison to the Ni-IM catalyst, the Ni-AE did not show any diffraction peak of crystalline Ni. Different from the catalysts after high-temperature stability test, no crystalline SiO_2 phase is detected after long-term stability test. In conclusion, the Ni particles of Ni-AE catalyst were quite stable under dry reforming reaction at 800 °C for 100 min and 700 °C for 100 h. The remarkable resistance to sintering for Ni-AE should be ascribed to the stabilized Ni particles by strong metal-support interactions. Therefore, the strong metal-support

interactions not only improved the resistance to coking, but also inhibited the particle sintering.

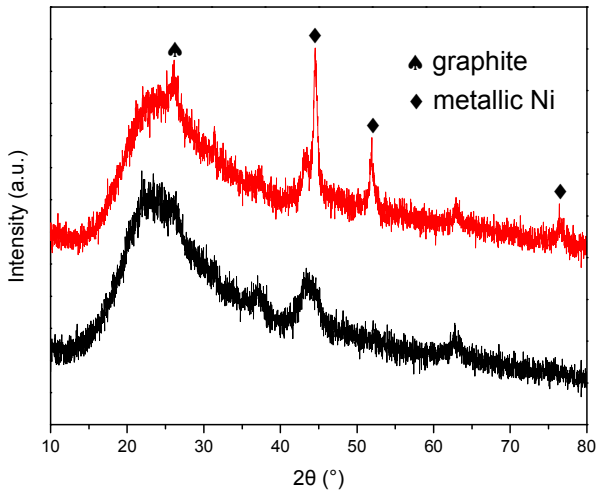

Fig. 12 Wide angle XRD patterns of the 100 h endurance-tested Ni/SBA-15 catalysts

4. Conclusion

Dry reforming of methane reaction was studied using the Ni/SBA-15 catalysts prepared by ammonia evaporation and impregnation method. Although both of the catalysts exhibited excellent initial catalytic activities of DRM, their high-temperature stability and long-term stability were very different resulting from the synthesis method. Compared with Ni-IM, the Ni-AE catalyst possessed smaller nickel particle size, higher dispersion and more uniform Ni particle distribution, which should be responsible for its excellent resistance to coking. The anchored Ni particles to the pore wall of SBA-15 derived from strong metal-support interactions was the main reason for stabilizing the catalysts against sintering. Hence, the AE method has potential applications in coking and sintering catalysts preparation for high-temperature hydrocarbon reforming reactions.

Acknowledgments

This work is supported by the National Natural Science Foundation of China (No.21307047, No.U1137603).

Notes and references

1 Y. H. Hu, E. Ruckenstein, Adv. Catal., 2004, **48**, 297.
2 M.C.J. Bradford, M.A. Vannice, Catal. Rev. Sci. Eng., 1999, **41**, 1.
3 D. Pakharea, J.Spivey, Chem. Soc. Rev., 2014, **43**, 7813.
4 P. Dokamaingam, N. Laosiripojana, A. Soottitantawat, S. Assabumrungrat, AIChE J., 2010, **56**, 1639.

5 J.R.H. Ross, Catal today, 2005. **100**. 151.
6 D.L. Trimm, Catal. Today, 1997, **37**, 233.
7 D.L. Trimm, Catal. Today, 1999, **49**, 3.
8 T.W. Hansen, A.T. DeLaRiva, S.R. Challa, A.K. Datye, Accounts Chem Res., 2013, **46**, 1720.
9 A.E.C. Luna, M.E. Iriarte, Appl. Catal., A., 2008, **343**, 10.
10 K.Y. Koo, H.-S. Roh, U.H. Jung, D. J. Seo, Y.-S. Seo, W.L. Yoon, Catal. Today, 2009, **146**, 166.
11 E. Ruckenstein, Y.H. Hu, Appl. Catal. A., 1995, 133, 149.
12 S. Therdthianwong, A. Therdthianwong, C. Siangchin, S. Yongprapat, Int J Hydrogen Energ., 2008, 33, 991.
13 D. Li, Y. Nakagawaa, K. Tomishige, Appl. Catal. A., 2011, 408, 1.
14 M. Yu, Y.-A. Zhu, Y. Lu, G. Tong, K. Zhu, X. Zhou, Appl. Catal. B., 2015, **165**, 43.
15 C. Shi, P. Zhang, Appl. Catal. B., 2012, **115-116**, 190.
16 A. Ungureanu, B. Dragoi, A. Chirieac, C. Ciotonea, S. Royer, D. Duprez, A.S. Mamede, E. Dumitriu, ACS Appl. Mater. Interfaces, 2013, **5**, 3010.
17 T. Ataloglou, J. Vakros, K. Bourikas, C. Fountzoula, C. Kordulis, A. Lycourghiotis, Appl. Catal., B., 2005, **57**, 299.
18 G.L. Bezemer, P.B. Radstake, V. Koot, A.J. van Dillen, J.W. Geus, K.P. de Jong, J. Catal. 2006, **237**, 291.
19 L.-F. Chen, P.-J. Guo, M.-H. Qiao, S.-R. Yan, H.-X. Li, W. Shen, H.-L. Xu, K.-N. Fan, J. Catal. 2008, **257**, 172.
20 A. Yin, J. Qu, X. Guo, W. Dai, K. Fan, Appl. Catal. A., 2011, **400**, 39.
21 A. Yin, C. Wen, X. Guo, W. Dai, K. Fan, J. Catal., 2011, **280**, 77.
22 A. Yin, X. Guo, W. Dai, K. Fan, J. Phys. Chem. C, 2009, **113**, 11003.
23 A. Yin, X. Guo, W. Dai, K. Fan, Appl. Catal. A., 2010, **377**, 128.
24 H. Yue, Y. Zhao, L. Zhao, J. Lv, S. Wang, J. Gong, X. Ma, AIChE J., 2012, **58**, 2798.
25 D. Zhao, J. Feng, Q. Huo, N. Melosn, G.H. Fredrickson, B.F. Chmelka, G.D. Stucky, Science, 1998, **279**, 548.
26 S. Chytil, W.R. Glomm, E.A. Blekkan, Catal. Today, 2009, **147**, 217.
27 A. Galarneau, M. Nader, F. Guenneau, F. Di Renzo, A. Gedeon, J. Phys. Chem. C, 2007, **111**, 8268.
28 C.J.G. van der Grift, P.A. Elberse, A. Mulder, J.W. Geus, Appl. Catal., 1990, **59**, 275.
29 P. Burattin, M. Che, C, Louis, J. Phys. Chem. B, 1997, **101**, 7060.
30 D. Liu, R. Lau, A. Borgna, Y. Yang, Appl. Catal. A., 2009, **358**, 110.
31 N. Wang, W. Chu, T. Zhang, X.S. Zhao, J. Hydrogen Energy, 2012, **37**, 19.
32 Y. Yang, S. Lim, G. Du, C. Wang, D. Ciuparu, Y. Chen, G.L. Haller, J. Phys. Chem. B, 2006, **110**, 5927.
33 Y. Yang, S. Lim, G. Du, Y. Chen, D. Ciuparu, G.L. Haller, J. Phys. Chem. B, 2005, **109**, 13237.
34 A.Mcdonald, B. Scott and G. Villemure, Micropor. Mesopor. Mat., 2009, **120**, 263.
35 P. Burattin, M. Che, C, Louis, J. Phys. Chem. B, 1997, **101**, 7060.
36 R. Gómez-Reynosoa, J. Ramírez, R. Nares, R. Luna, F. Murrieta, Catal. Today, 2005, **107-108**, 926.
37 J.W.E. Coenen, Appl. Catal., 1991, **75**, 193.
38 M.E. Bertone, C.I. Meyer, S.A. Regenhardt, V. Sebastian, T.F. Garetto, A.J. Marchi, Appl. Catal. A., 2015, **503**, 135.

39 M. Montes, Ch. Penneman de Bosscheyde, B.K. Hodnett, F. Delannay, P. Grange, B. Delmon, Appl. Catal., 1984, **12**, 309.
40 D.G. Blackmond, E.I.Ko, Appl. Catal., 1984, **13**, 49.
41 S. Uchiyama, Y. Obayashi, T. Hayasaka, N. Kawata, Appl. Catal., 1989, **47**, 155.
42 M. A. Keane, P.M. Patterson, J. Chem. Soc., Faraday Trans., 1996, **92**, 1413.
43 Q. Zhang, T. Wu, P. Zhang, R. Qi, R. Huang, X. Song, L. Gao, RSC Adv., 2014, **4**, 51184.
44 J. A. Moulijn, A. E. van Diepen, F. Kapteijn, Appl. Catal. A., 2001, **212**, 3.
45 D. Liu, X.Y. Quek, W.N.E. Cheo, R. Lau, A. Borgna, Y. Yang, J. Catal., 2009, **266**, 380.
46 L. Xu, J. Zhang, F. Wang, K. Yuan, L. Wang, K. Wu, G. Xu, W. Chen, RSC Adv., 2015, **5**, 48256.
47 S. Damyanova, B. Pawelec, K. Arishtirova, J.L.G. Fierro, C. Sener, T. Dogu, Appl. Catal. B., 2009, **92**, 250.
48 S.M. de Lima, A.M. da Silva, L.O.O. da Costa, U.M. Graham, G. Jacobs, B.H. Davis, L.V. Mattos, F.B. Noronha, J. Catal., 2009, **268**, 268.
49 A.E. Castro Luna, M.E. Iriarte, Appl. Catal. A., 2008, **343**, 10.
50 S. Helveg, C. Lòpez-Cartes, J. Sehested, P.L. Hansen, B.S. Clausen, J.R. Rostrup-Nielsen, F. Abild-Pedersen, J.K. Nørskov, Nature, 2004, **427**, 426.
51 W. Donphai, K. Faungnawakij, M, Chareonpanich, J. Limtrakul, Appl. Catal. A., 2014, **475**, 16.
52 L. Xu, H. Song, L. Chou, ACS Catal., 2012, **2**, 1331.
53 Q. Zhang, T. Wu, P. Zhang, R. Qi, R. Huang, X. Song, L. Gao, RSC Adv., 2014, **4**, 51184.

Graphical Abstract

A stable Ni/SBA-15 catalyst prepared by the ammonia evaporation method for dry reforming of methane

Qiulin Zhang*, Mingzhi Wang, Tengfei Zhang, Yiru Wang, Xiaosu Tang, Ping Ning

Faculty of Environmental Science and Engineering, Kunming University of Science and Technology. Kunming, 650500, P.R. China

* Corresponding author. E-mail: qiulinzhang_kmust@163.com

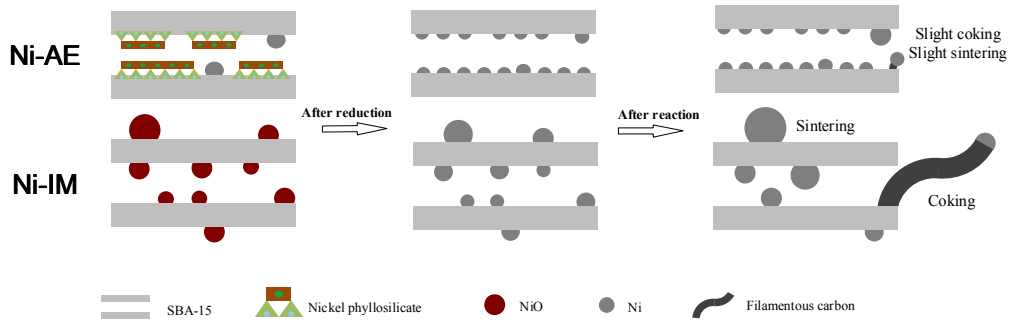

Coking and sintering were inhibited simultaneously by the strong metal-support interactions.